NUMERICAL STUDY OF NORMAL PRESSURE DISTRIBUTION IN ENTRANCE PIPE FLOW[*]

K. SHIMOMUKAI[†] AND H. KANDA[‡]

Abstract. This paper deals with the computation of pipe flow in the entrance region. The pressure distribution and flow characteristics, particularly the effect of vorticity in the vicinity of the wall, are analyzed for Reynolds numbers (Re) ranging from 500 to 10000. The pressure gradient in the normal or radial direction is caused by the normal component of the curl of vorticity, which decreases as Re increases. It is found, for the first time, that the pressure gradient along the normal direction near the pipe inlet is negative, i.e., the pressure at the wall is lower than that at the central core for Re $\leq$ 5000. This result is beyond the scope of the boundary-layer assumption and contrary to the consequence of Bernoulli's law.

Key words. computational fluid dynamics, numerical analysis

AMS subject classifications. 15A15, 15A09, 15A23

1. Introduction.

1.1. Background and objectives. Numerous investigations of laminar incompressible fluid flow along the entrance region of a smooth circular pipe have been made both experimentally and theoretically since the work of Hagen in 1839 and Poiseuille in 1841. Shah and London [19] presented an excellent overall review of previous research studies on such problems. Generally, thus far, three major variables have been studied [6]: (i) the velocity distribution in all sections, (ii) the entrance length (Le), and (iii) the pressure difference between any two sections. The results of previous research studies on the velocity distribution, entrance length, and pressure difference in dimensionless X coordinates are approximately the same at Reynolds numbers Re $\geq$ 500, i.e., these quantities are independent of the Reynolds number for Re $\geq$ 500 [3].

Up to now, the problem of transition between laminar and turbulent flows in a pipe has not yet been solved. Since Reynolds discovered the laminar-turbulent transition problem in 1883, the transition occurs necessarily in the pipe entrance region at Re approximately $\geq$ 2000 [21].

Therefore, the first objective of this investigation is to find and confirm a variable or parameter that varies as the Reynolds number increases in order to enable flow stability studies [10]. To this end, we found, in the previous study of channel flow, that there is a significant difference between the pressure p_w at the wall and p_c at the centerline in the normal or radial direction, that decreases as Re increases [20].

It is convenient for computational purposes, to divide the flow region into the entrance region and the developed region. In the entrance region, the mass flux transported along the pipe remains the same across each cross section. Since the streamwise velocities near the wall are retarded by shearing stresses, the velocities at the central parts near the axis must increase until, finally, an equilibrium condition is established between the pressure drop and the shear stresses. Accordingly, our assumed uniform velocity profile at the inlet is gradually transformed, because of viscous forces, into the well–known parabolic, Poiseuille-type distribution downstream. We denote by "fully developed region", the downstream region

[†] Department of Visualization, SGI Japan, Ltd., Yebisu Garden Place Tower 31F, 4-20-3 Ebisu Shibuya-ku, Tokyo 150-6031, Japan (shimomukai@sgi.co.jp).

[‡]Department of Computer Science, University of Aizu, Aizu-Wakamatsu, Fukushima 965-8580, Japan (kanda@u-aizu.ac.jp).

after the entrance length; in this region, the velocity distribution and the pressure drop per unit axial distance are constant.

All of the foregoing solutions involve the boundary-layer assumptions, i.e., the axial diffusion of momentum and normal pressure gradient are neglected; see [2, 4] in Subsection 1.2. Prandtl's boundary-layer assumption is that the pressure inside the boundary layer is the same as that outside the boundary layer in the radial direction. It has been successfully applied for flows with high Reynolds numbers in many fluid dynamics studies. Moreover, it was applied to theoretical investigations of pipe flow, in which pressure was assumed to be a function of the axial distance only and one-dimensional. Hence, we must numerically investigate the reason why the pressure gradient, $\partial p/\partial r$, is negative near the wall of the entrance region.

Peyret and Taylor [15] state that the two most troublesome boundary conditions to prescribe and satisfy are
(i) the downstream flow conditions and
(ii) the pressure conditions at a solid surface.
Our second objective, thus, is to develop a more accurate algorithm for the calculation of the pressure distribution, without making any assumptions about the pressure distribution at the wall.

1.2. Literature review. Very little is known about the radial pressure gradient [9]. Generally, solutions of the Navier-Stokes (N-S) equations for pipe entrance flow consist of approximate solutions of restricted forms of the N-S equations, variations in the applications of the boundary-layer equations, or combinations of these in which a boundary-layer solution valid near the inlet is coupled with a restricted equation of motion that is valid far from the inlet.

Let us here consider previous analyses and assumptions [2, 4, 12]. By restricting the applications of the N-S equations in cylindrical coordinates such that:
(i) the flow is in a steady state,
(ii) the radial component of the N-S equations is negligible, and
(iii) the angular motion (i.e., the axisymmetric flow) is negligible, then the N-S equations can be simplified as follows:

$$(1.1) \qquad 2\left(u\frac{\partial u}{\partial x} + v\frac{\partial u}{\partial r}\right) \;=\; -\frac{\partial p}{\partial x} \;+\; \frac{2}{Re}\left[\frac{1}{r}\frac{\partial}{\partial r}\left(r\frac{\partial u}{\partial r}\right) + \frac{\partial^2 u}{\partial x^2}\right].$$

One or more of the following additional assumptions were made by others for obtaining solutions to (1.1):
(iv) The axial transport of momentum is negligible, i.e., mathematically,

$$\frac{\partial^2 u}{\partial x^2} \;\ll\; \frac{1}{r}\frac{\partial}{\partial r}\left(r\frac{\partial u}{\partial r}\right);$$

(v) The axial velocity at the pipe inlet is uniform: $u|_{x=0} = U_0 = 1$;
(vi) The effect of radial flow is negligible;

$$v\frac{\partial u}{\partial r} \;\ll\; u\frac{\partial u}{\partial x}.$$

(vii) The pressure is a function of x and is independent of r; and
(viii) The pressure is obtained by integrating

$$-\frac{\partial p}{\partial x} \;=\; 2u\frac{\partial u}{\partial x}\bigg|_{x=0}.$$

1.3. Nomenclature.

D	=	pipe diameter
I_0	=	maximum axial point of mesh system
i	=	axial point of mesh system
J_0	=	maximum radial point of mesh system
j	=	radial point of mesh system
Le	=	dimensionless entrance length = $x_e'/(DRe)$
p	=	dimensionless static pressure = $p'/((1/2)\rho U_0^2)$
p_c	=	dimensionless static pressure at centerline
p_w	=	dimensionless static pressure at wall
p'	=	static pressure
r	=	dimensionless radial coordinate = r/D
r'	=	radial coordinate
R	=	dimensionless pipe radius = $R'/D = 0.5$
R'	=	pipe radius
Re	=	Reynolds number based on pipe diameter = $U_0 D/\nu$
t	=	dimensionless time = $(U_0/D)t'$
t'	=	time
u	=	axial velocity
U_0	=	average axial velocity = 1
v	=	radial velocity
V	=	velocity vector
x	=	dimensionless axial coordinate = x'/D
x'	=	axial coordinate
x_e'	=	actual entrance length
X	=	dimensionless axial coordinate = $x'/(DRe) = x/Re$
ψ	=	dimensionless streamfunction = $\psi'/(U_0 D^2)$
ψ'	=	streamfunction
ω	=	dimensionless vorticity = $(D/U_0)\omega'$
ω'	=	vorticity
θ	=	angle in cylindrical coordinates
ν	=	kinematic viscosity
ρ	=	fluid density
$\triangle p$	=	axial pressure drop from the inlet
$\triangle r$	=	radial mesh size
$\triangle x$	=	axial mesh size

2. Governing equations. Figure 2.1 is a two dimensional plot of normalized entrance length against normalized radius of the pipe, with pipe radius r in the range $0 \le r \le 0.5$. The setup comprises a smooth, straight, circular pipe without a bellmouth at the pipe inlet. We have assumed that at the inlet $x = 0$, the fluid enters the pipe with a flat axial velocity profile U_0 across the pipe, and that there is no velocity component in the radial direction.

First, we consider dimensionless variables. All lengths and velocities are normalized by the pipe diameter D and the mean velocity U_0, respectively. The pressure is normalized by $(1/2)\rho U_0^2$. The Reynolds number is based on the pipe diameter and the mean velocity. Note that the dimensionless axial coordinate x ($= x'/D$) is used for calculation and X ($= x'/(DRe)$) is used for the presentation of our figures and tables; x' is the actual axial coordinate.

2.1. Governing equations. We consider unsteady flow of an incompressible Newtonian fluid with constant viscosity and density, and we disregard gravity and external forces. Our aim is to initially eliminate the appearance of the pressure term in the equations, and to this
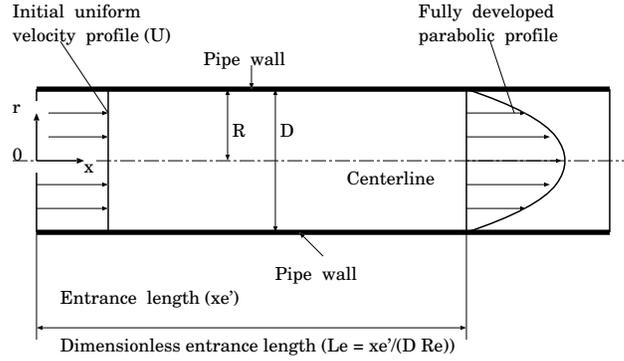
FIG. 2.1. *Velocity development in entrance region.*

end, we introduce streamfunction and vorticity formulae in two-dimensional coordinates to enable computation of the velocity components without any assumptions on the pressure. We can later compute the pressure distribution using computed values of the velocity.

The transport equation for the vorticity written in dimensionless form [14] is the equation

$$(2.1) \quad \frac{\partial \omega}{\partial t} - \frac{1}{r} \frac{\partial \psi}{\partial x} \frac{\partial \omega}{\partial r} + \frac{1}{r} \frac{\partial \psi}{\partial r} \frac{\partial \omega}{\partial x} + \frac{\omega}{r^2} \frac{\partial \psi}{\partial x} = \frac{1}{Re} \left[\frac{\partial}{\partial r} \left\{ \frac{1}{r} \frac{\partial (r\omega)}{\partial r} \right\} + \frac{\partial^2 \omega}{\partial x^2} \right].$$

The Poisson equation for ω is derived from the definition of ω, i.e.,

$$(2.2) \quad -\omega = \nabla^2 \psi = \frac{\partial}{\partial r} \left(\frac{1}{r} \frac{\partial \psi}{\partial r} \right) + \frac{\partial^2}{\partial x^2} \left(\frac{\psi}{r} \right).$$

The axial velocity u and radial velocity v are defined as derivatives of the streamfunction, i.e.,

$$(2.3) \quad u = \frac{1}{r} \frac{\partial \psi}{\partial r}, \quad v = -\frac{1}{r} \frac{\partial \psi}{\partial x}.$$

Only the angular (i.e., θ) component of a two-dimensional flow field ω is non-negligible, and we shall thus write ω for $\omega(\theta)$, i.e.,

$$(2.4) \quad \omega = \omega_\theta = [\nabla \times V]_\theta = \frac{\partial v}{\partial x} - \frac{\partial u}{\partial r}.$$

The ψ–ω solution does not give any information regarding the pressure field. The pressure can be calculated using the steady-state form of the N-S equations [14]. The pressure distribution for the x derivative is

$$(2.5) \quad \frac{\partial p}{\partial x} = -2 \left(u \frac{\partial u}{\partial x} + v \frac{\partial u}{\partial r} \right) + \frac{2}{Re} \left(\frac{\partial^2 u}{\partial x^2} + \frac{1}{r} \frac{\partial u}{\partial r} + \frac{\partial^2 u}{\partial r^2} \right),$$

and that for the r derivative is

$$(2.6) \quad \frac{\partial p}{\partial r} = -2 \left(u \frac{\partial v}{\partial x} + v \frac{\partial v}{\partial r} \right) + \frac{2}{Re} \left(\frac{\partial^2 v}{\partial x^2} + \frac{1}{r} \frac{\partial v}{\partial r} - \frac{v}{r^2} + \frac{\partial^2 v}{\partial r^2} \right).$$

Since u and v are known at every point, from (2.3), the derivatives on the right-hand sides of (2.5) and (2.6) can be computed. Hence, note that the result of (2.5) must satisfy the result
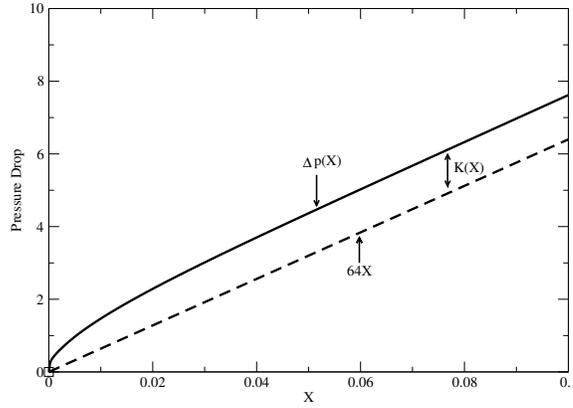
FIG. 2.2. *Development of pressure drop in pipe flow.*

of (2.6). Accordingly, a smooth pressure distribution that satisfies both (2.5) and (2.6) is calculated using Poisson's equation [18],

$$
(2.7) \qquad \nabla^2 p \;=\; \frac{\partial^2 p}{\partial x^2} + \frac{\partial^2 p}{\partial r^2} + \frac{1}{r}\frac{\partial p}{\partial r} \;=\; \frac{1}{r}\left[\frac{\partial}{\partial x}\left(r\frac{\partial p}{\partial x}\right) \;+\; \frac{\partial}{\partial r}\left(r\frac{\partial p}{\partial r}\right)\right]
$$

$$
\;=\; -2\left[\left(\frac{\partial v}{\partial r}\right)^2 + 2\frac{\partial u}{\partial r}\frac{\partial v}{\partial x} + \left(\frac{\partial u}{\partial x}\right)^2 + \frac{v^2}{r^2}\right].
$$

Note that from (2.7), the pressure itself is determined only by the velocities and is independent of the Reynolds number. In this study, initial values are obtained using (2.5), and then (2.7) is used to obtain better solutions.

2.2. Axial pressure drop at centerline. For fully developed flow where $\partial p/\partial r = 0$, the pressure gradient at the centerline [24] is given by

$$
-\frac{dp}{dx} \;=\; \frac{64}{Re}.
$$

The total pressure drop $\triangle p(X)$ from the pipe inlet is expressed as the sum of the pressure drop that would occur if the flow were fully developed, plus the excess pressure drop $K(X)$ to account for the developing region,

$$
(2.8) \qquad \triangle p(X) \;=\; p(0) \;-\; p(X) \;=\; -p(X) \;=\; 64X \;+\; K(X).
$$

The pressure drop can be conveniently represented by (2.8), as shown in Figure 2.2.

2.3. Normal pressure gradient at wall. Here, we consider the normal pressure gradient $\partial p/\partial r$. The dimensionless N-S equation in vector form [6] is written as

$$
(2.9) \qquad \frac{\partial V}{\partial t} - V \times \omega = -\frac{1}{2}grad\,(p + V^2) - \frac{1}{Re}\nabla \times \omega.
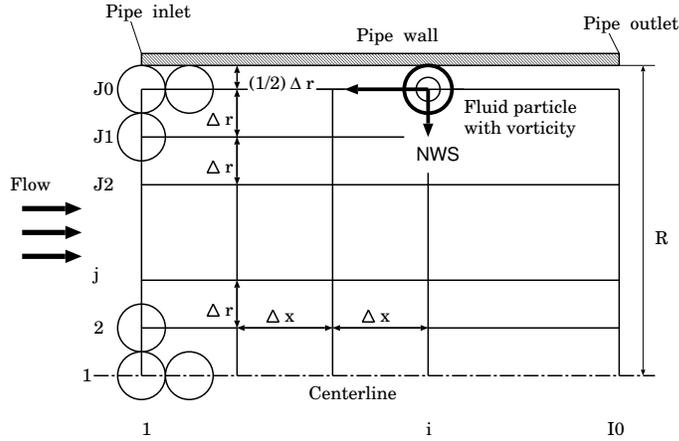$$

FIG. 2.3. *Direction of curl of vorticity on wall.*

Since the velocity vector $V = 0$ at the wall, that is, the normal component of (2.9) at the wall, reduces to

$$(2.10) \qquad \left.\frac{\partial p}{\partial r}\right|_{r=R} = -\frac{2}{Re}\left.\nabla \times \omega\right|_{r=R} = \left.\frac{2}{Re}\frac{\partial \omega_\theta}{\partial x}\right|_{r=R},$$

the normal pressure gradient is derived from the negative normal component of the curl of vorticity at the wall. This normal pressure gradient is also presented as

$$(2.11) \qquad \frac{\partial p}{\partial n} = -\left.\frac{2}{Re}\frac{\partial \omega_\theta}{\partial s}\right|_{r=R},$$

where (n, s) are the normal and tangent to the wall [18]. Since $n = -r$ and $s = x$ at the wall, (2.10) and (2.11) are the same. Equation (2.10) is, however, clearer than (2.11) when we consider a physical force mechanism in vector form. The normal component of the curl of vorticity at the wall hereafter is called the normal wall strength (NWS). From (2.10), NWS is expressed as

$$(2.12) \qquad NWS \equiv \left.\frac{2}{Re}\nabla \times \omega\right|_{r=R} = -\left.\frac{2}{Re}\frac{\partial \omega_\theta}{\partial x}\right|_{r=R} = -\left.\frac{\partial p}{\partial r}\right|_{r=R}.$$

The following characteristics of NWS are considered.

(i) NWS is effective near the pipe inlet where the vorticity gradient in the x-direction is large and decreases inversely with the Reynolds number. In the fully developed region, NWS vanishes, since the curl of vorticity disappears.

(ii) It is clear from (2.12) that NWS causes a pressure gradient in the radial direction, that is, the pressure gradient at the wall results from the curl of vorticity. NWS and the normal pressure gradient $\partial p/\partial r$ have the same magnitude at the wall, but have opposite directions. When $\partial p/\partial r < 0$, the direction of NWS is from the wall to the centerline, as shown in Figure 2.3. NWS causes the fluid particles near the wall to move towards the centerline in the normal direction.

(iii) When using the boundary-layer assumptions, NWS vanishes since $\partial p/\partial r$ is always neglected in the assumptions.

3. Numerical methods. The rectangular mesh system used is schematically shown in Figure 2.3, where $I0$ and $J0$ are the maximum numbers of mesh points in the x- and r-directions, respectively, and $I1 = I0 - 1$, $I2 = I0 - 2$, $J1 = J0 - 1$, and $J2 = J0 - 2$.

In this paper, generally, $I0 = 1001$ and $J0 = 101$. The dimensionless $\triangle X = 0.0001$ grid space is used for calculations of Le and $K(\infty)$ (see Subsection 4.2); since $\triangle x = \triangle X \times Re$, $\triangle x$ and the maximum x-distance, $x = (I0 - 1)\triangle x$, are proportional to Re. On the other hand, the $\triangle X = 0.00001$ grid space is used for calculations of the pressure distribution in the radial direction; see Subsection 4.3.

3.1. Vorticity transport equation. This computational scheme involves the forward-time, center-space (FTCS) method. For unsteady problems, (2.1) in finite difference form can be solved efficiently in time using an explicit [8, 9] or implicit Gauss-Seidel iteration method (this study). The implicit form for vorticity is written as

$$(3.1) \qquad \frac{\omega^{n+1} - \omega^n}{\triangle t} - \frac{1}{r}\frac{\partial \psi^n}{\partial x}\frac{\partial \omega^{n+1}}{\partial r} + \frac{1}{r}\frac{\partial \psi^n}{\partial r}\frac{\partial \omega^{n+1}}{\partial x} + \frac{\omega^{n+1}}{r^2}\frac{\partial \psi^n}{\partial x}$$

$$= \frac{1}{Re}\left[\frac{\partial}{\partial r}\left\{\frac{1}{r}\frac{\partial(r\omega^{n+1})}{\partial r}\right\} + \frac{\partial^2\omega^{n+1}}{\partial x^2}\right],$$

where n corresponds to the time step.

Consider the initial streamfunction. From (2.3), the initial condition for the streamfunction is given by

$$\psi(i,j) = \frac{1}{2}[(j-1)\triangle r]^2, \quad 1 \le i \le I0, \quad 1 \le j \le J0,$$

where (i,j) is the axial point and radial point of the mesh system; see Figure 2.3. Within the boundaries, the initial vorticity is obtained by solving (2.2). The velocities u and v are set using (2.3) whenever the streamfunction is newly calculated.

The following are the boundary conditions.
(i) At the centerline: $\psi_{i,1} = 0$, $\omega_{i,1} = 0$, $1 \le i \le I1$.
(ii) At the inlet: $\psi_{1,j} = 0.5[(j-1)\triangle r]^2$, $\omega_{1,j} = 0$, $2 \le j \le J1$.
(iii) At the wall: $\psi_{i,J0} = 0.5[(J0-1)\triangle r]^2$, $1 \le i \le I1$.
The vorticity boundary condition at no-slip walls is derived from (2.4) to be

$$(3.2) \qquad\qquad \omega = -\frac{\partial u}{\partial r}.$$

A three-point, one-sided approximation for (3.2) is used to maintain second-order accuracy:

$$(3.3) \qquad \omega_{i,J0} \approx -\frac{3u_{i,J0} - 4u_{i,J1} + u_{i,J2}}{2\triangle r} = \frac{4u_{i,J1} - u_{i,J2}}{2\triangle r}.$$

(iv) At the outlet, the linear extrapolation method is used: $\psi_{I0,j} = 2\psi_{I1,j} - \psi_{I2,j}$, $\omega_{I0,j} = 2\omega_{I1,j} - \omega_{I2,j}$, $1 \le j \le J0$.

3.2. Pressure distribution. The following are the boundary conditions for pressure.
(i) For the pressure at the centerline, we use the three-point finite difference form; since $\partial p/\partial r = 0$ at $r = 0$,

$$p_{i,1} = \frac{4p_{i,2} - p_{i,3}}{3}, \quad 1 \le i \le I0.$$

TABLE 4.1
Effects of mesh system on velocity development at Re = 2000

Case	case 1	case 2	case 3	case 4	case 5	case 6	case 7	case8
I0	11	21	31	51	101	201	1001	10001
J0	11	21	31	51	101	201	101	101
T-steps ($\times 10^3$)	200	300	400	400	500	1600	6200	12,000
CPU [s]	870	4890	6370	11,280	12,370	26,340	248,900	2,003,830
X				Velocity development				
0.00001	–	–	–	–	–	–	–	1.0067
0.00003	–	–	–	–	–	–	–	1.0198
0.00005	–	–	–	–	–	–	–	1.0324
0.0001	–	–	–	–	–	–	1.0770	1.0606
0.0003	–	–	–	–	–	–	1.1513	1.1225
0.0005	–	–	–	–	–	–	1.1809	1.1526
0.001	–	–	–	–	1.2530	1.2515	1.2286	1.2059
0.003	–	–	–	–	1.3823	1.3732	1.3532	1.3389
0.005	–	1.4631	–	–	1.4673	1.4581	1.4413	1.4300
0.01	1.5932	1.6284	1.6321	1.6300	1.6228	1.6152	1.6037	1.5959
0.03	1.8778	1.9024	1.9055	1.9057	1.9036	1.9014	1.8993	1.8973
0.05	1.9499	1.9712	1.9741	1.9748	1.9743	1.9736	1.9732	1.9727
0.056	–	–	–	1.9829	1.9827	1.9822	1.9819	1.9816
0.07	1.9689	1.9891	1.9920	1.9930	1.9930	1.9928	1.9927	1.9926
0.1	1.9753	1.9947	1.9976	1.9987	1.9990	1.9990	1.9982	1.9989
$Le(99\%)$	–	0.0569	0.0542	0.0536	0.0538	0.0543	0.0545	0.0547
$K(\infty)$	1.453	1.342	1.274	1.217	1.176	1.157	1.220	1.270

(ii) The pressure at the inlet is given as zero throughout the $p_{1,j} = 0, \quad 1 \le j \le J1$.
(iii) The pressure at the wall is derived from (2.10). For the leading edge at $x = 0$ $(i = 1)$ and
$r = R$ $(j = J0)$, the following three-point approximation is used for p and ω. The pressure
gradient is expressed as

$$\left.\frac{\partial p}{\partial r}\right|_{i=1,j=J0} \approx \frac{3p_{1,J0} - 4p_{1,J1} + p_{1,J2}}{2\triangle r} = \frac{2}{Re}\left(\frac{-\omega_{3,J0} + 4\omega_{2,J0} - 3\omega_{1,J0}}{2\triangle x}\right).$$

For the wall with $2 \le i \le I1$ and $J = J0$,

$$\left.\frac{\partial p}{\partial r}\right|_{i\ge2,j=J0} \approx \frac{3p_{i,J0} - 4p_{i,J1} + p_{i,J2}}{2\triangle r} = \frac{2}{Re}\left(\frac{\omega_{i+1,J0} - \omega_{i-1,J0}}{2\triangle x}\right).$$

(iv) The following linear extrapolation method is used for the outflow boundary conditions:
$p_{I0,j} = 2p_{I1,j} - p_{I2,j}, \quad 1 \le j \le J0$.

4. Results and discussion. The numerical calculations were carried out on an NEC
SX-7/232H32 supercomputer that has a peak performance of 8.83 G-FLOPS/processor. CPU
times are listed in Table 4.1, including the number of $I0 \times J0$ and the time steps required
to reach a steady-state solution (with maximum n in (3.1)). The calculations were actually
performed using four parallel processors, so that the actual CPU times were one-quarter of
the listed values.

In order to check the accuracy, numerical calculations were performed for 8 different
mesh spacings from 11×11 (case 1) to 10001×101 (case 8), as listed in Table 4.1. It is clear,
judging from the Le value at $X = 0.1$, that the calculated results of Le are approximately the
same for mesh systems of above 21×21.

Moreover, to evaluate the accuracy of calculations, the calculated velocity development,
entrance length, and excess pressure drop were compared with those obtained by the previous
researchers. The accuracy of the calculations in this study was thus verified, as described in
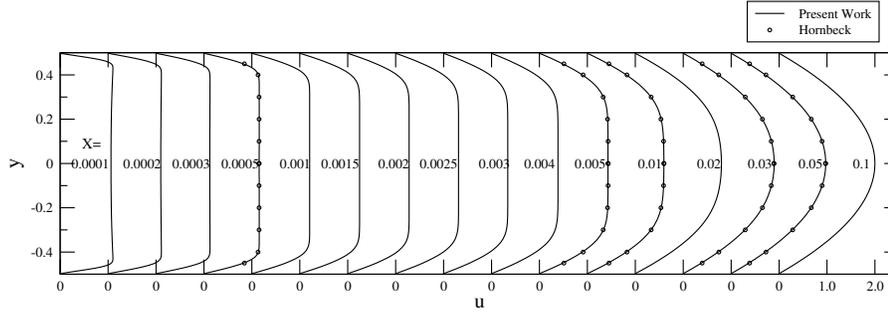the following subsections.

FIG. 4.1. *Velocity profile of axial velocity component at Re = 2000.*

TABLE 4.2
Velocity development at Re = 2000 for 10001 × 101 mesh system (case 8)

X	r=0	r=0.1	r=0.2	r=0.3	r=0.4	r=0.45	p_c	p_w
0.00001	1.0067	1.0069	1.0079	1.0106	1.0206	1.0420	-0.0193	-0.0217
0.00003	1.0198	1.0205	1.0233	1.0306	1.0544	1.0908	-0.0312	-0.2210
0.00005	1.0324	1.0336	1.0378	1.0480	1.0751	1.1015	-0.0518	-0.2067
0.0001	1.0606	1.0622	1.0675	1.0781	1.0959	1.0766	-0.1000	-0.1885
0.0003	1.1225	1.1229	1.1239	1.1254	1.1248	0.9369	-0.2198	-0.2307
0.0005	1.1526	1.1527	1.1530	1.1534	1.1367	0.8500	-0.2864	-0.2893
0.001	1.2059	1.2059	1.2060	1.2060	1.1142	0.7273	-0.4114	-0.4119
0.003	1.3389	1.3389	1.3385	1.3112	0.9797	0.5632	-0.7494	-0.7487
0.005	1.4300	1.4299	1.4238	1.3369	0.9078	0.5063	-1.0015	-1.0006
0.01	1.5959	1.5897	1.5401	1.3322	0.8245	0.4480	-1.5085	-1.5075
0.03	1.8973	1.8407	1.6521	1.2933	0.7419	0.3941	-3.0609	-3.0599
0.05	1.9727	1.8988	1.6725	1.2833	0.7256	0.3836	-4.4160	-4.4150
0.056	1.9816	1.9056	1.6748	1.2822	0.7238	0.3824	-4.8113	-4.8103
0.07	1.9926	1.9140	1.6777	1.2807	0.7214	0.3809	-5.7254	-5.7244
0.1	1.9989	1.9189	1.6794	1.2799	0.7201	0.3801	-7.6696	-7.6686
				Hornbeck [7]				
0.0005	1.1503	1.1503	1.1503	1.1502	1.1293	0.8434	-0.3220	–
0.005	1.4332	1.4324	1.4214	1.3292	0.9107	0.5102	-1.0506	–
0.01	1.5977	1.5893	1.5358	1.3308	0.8261	0.4496	-1.5610	–
0.03	1.8920	1.8366	1.6509	1.2943	0.7429	0.3947	-3.1064	–
0.05	1.9698	1.8969	1.6721	1.2840	0.7263	0.3840	-4.4520	–

4.1. Velocity development. The calculated results of axial velocity development for case 8 (mesh system of size 10001×101 in Table 4.1 are shown in Figure 4.1 and the details are listed in Table 4.2. The circles show the velocity profiles given by Hornbeck [7]. The results for our 10001×101 mesh agree well with those obtained by Hornbeck, although Hornbeck solved the problem numerically with the $(250+\alpha) \times (10+\alpha)$ mesh system. Note that in Figure 4.1 and Table 4.2, the velocity distribution is concave in the central portion for $X \leq 0.0002$ at Re = 2000, as Wang and Longwell found for channel flow [23], and Vrentas et al. found for pipe flow [22].

4.2. Entrance length and excess pressure drop. The entrance length, which is defined as the distance from the inlet to the point where the centerline velocity reaches 99% of the fully developed pipe flow ($u_{|r=0} = 1.98$), is expressed by Chen [3] as

$$(4.1) \qquad Le = \frac{x_e{}'}{DRe} = \frac{0.60}{Re(0.035Re + 1)} + 0.056.$$

From (4.1), Le = 0.0573 at Re = 100, 0.0562 at Re = 300, and 0.0561 at Re = 400, whereas Le takes a constant value of 0.056 at $X \geq 500$.

TABLE 4.3
Entrance length Le and excess pressure drop $K(\infty)$

Author	Year	$Le(99\%)$	$K(\infty)$	I0	J0	Note
		Experiment				
Rieman [17]	1928	–	1.248	–	–	–
Reshotko [16]	1958	0.06	–	–	–	Re=7600
Leite [13]	1959	0.052	–	–	–	Re=13000
		Analytical				
Atkinson & Goldstein [1]	1938	0.06	1.41	–	–	–
Langhaar [12]	1942	0.0568	1.28	–	–	–
Chen [3]	1973	0.056	1.219	–	–	Re=2000
		Numerical				
Hornbeck [7]	1964	0.0565	1.280	250+α	10+α	
Christiansen & Lemmon [4]	1965	0.0555	1.274	200	200	With radial term
Vrentas et al. [22]	1966	0.0535	1.28	20	20	Complete Eqs.
Vrentas et al. [22]	1966	0.0563	1.18	20	20	Boundary-layer
Kanda [8]	1986	0.055	–	150	21	Re>50
Durst et al. [5]	2005	0.0565	–	400	80	Re=1000
Present result (a)	2007	0.0544	1.217	1001	101	Re=500
$\triangle X = 0.0001$	2007	0.0545	1.218	1001	101	Re=1000
	2007	0.0545	1.220	1001	101	Re=2000
	2007	0.0545	1.220	1001	101	Re=3000
	2007	0.0544	1.221	1001	101	Re=5000
	2007	0.0544	1.221	1001	101	Re=10000
Present result (b)	2007	0.0547	1.270	10001	101	Re=2000
$\triangle X = 0.00001$	2007	0.0547	1.266	10001	101	Re=10000

If the axial distance X is longer than the entrance length Le, $K(X)$ is assumed to be $K(\infty)$ for the fully developed region. Chen [3] obtained expression (4.2) for $K(\infty)$. From (4.2), $K(\infty)$ is 1.219 at Re = 2000 and 1.204 at Re = 10000,

$$(4.2) \qquad K(\infty) \;=\; 1.20 \;+\; \frac{38}{Re}.$$

Our calculated values of Le and $K(\infty)$ are listed in Table 4.3. We studied the effects of (a) the mesh system and (b) the Reynolds number on Le and $K(\infty)$.

The following are our main calculated results.

(i) We see, from case 1 for an 11×11 mesh in Table 4.1, that Le was unable to reach 99% of its fully developed value ($u|_{r=0}$=1.98) even at $X = 0.1$, and that u at the centerline and X=0.1 was 1.9753. Le reached 99% of its limiting value at around $X = 0.054 - 0.057$ for meshes finer than 21×21. The value of $K(\infty)$ decreases as the mesh system becomes more refined, e.g., from 1.447 for an 11×11 mesh, to 1.157 for a 201×201 mesh (see case 2-6).

(ii) In the present results concerning (a) in Table 4.3 with $\triangle X = 0.0001$, we obtained a near constant value of Le in the range 0.0544–0.0545 for all Re $\geq$ 500. Our computed value of $K(\infty)$ attained an approximately constant value in the range 1.217-1.221 for all Re $\geq$ 500. Our results thus agree well with those predicted using (4.2).

(iii) For the refined mesh with $\triangle X = 0.00001$ (present results for (b) in Table 4.3), the value of Le is 0.0547, which is equal to that in the present results for (a) in Table 4.3. The value of $K(\infty)$, however, is 1.266-1.270, which is slightly larger than that in the present results for (a).

4.3. Radial pressure distribution. Let us now discuss the value of the pressure as a function of radial distance from the centerline, that is, as a function of r, where $p_c = p(0)$ denotes the pressure at the centerline, and $p(R) = p_w$ denotes the pressure at the wall. We first examine this issue symbolically, via our difference approximation. Since the axial velocity $u_{i,J0}$ is zero at the wall, the x component of velocity, u, can be approximately linear

as follows:

$$(4.3) \qquad u_{i,J1} \approx \frac{(u_{i,J0} + u_{i,J2})}{2} = \frac{1}{2} u_{i,J2}.$$

From (3.2), (3.3), and (4.3), the vorticity at the wall is simply approximated as follows:

$$(4.4) \qquad \omega_{i,J0} = -\frac{\partial u}{\partial r}\bigg|_{r=R} \approx \frac{u_{i,J1}}{\triangle r} > 0.$$

Substituting (4.4) into (2.10) gives

$$(4.5) \qquad \frac{\partial p}{\partial r}\bigg|_{r=R} = \frac{2}{Re} \frac{\partial \omega_\theta}{\partial x}\bigg|_{r=R}$$

$$\approx \frac{2}{Re} \frac{\partial}{\partial x}\left(\frac{u_{i,J1}}{\triangle r}\right) \approx \frac{2}{Re}\left(\frac{u_{i+1,J1} - u_{i-1,J1}}{2\triangle x \triangle r}\right) \leq 0.$$

Since $u_{i+1,J1} < u_{i-1,J1}$ in the entrance region, the normal pressure gradient at the wall is negative. It thus follows from (4.5) that pressure gradient in the radial direction is negative at the wall of the entrance region.

On the other hand, the normal pressure gradient at the wall of the fully developed region becomes 0, so that the pressure distribution becomes constant in the radial direction. The velocity in the fully developed region is given by

$$(4.6) \qquad u(r) = 2\left(1 - \frac{r^2}{R^2}\right).$$

Differentiating (4.6) with respect to r gives

$$\omega|_{r=R} = -\frac{\partial u}{\partial r}\bigg|_{r=R} = -2\left(-\frac{2R}{R^2}\right) = 4\frac{1}{R} = 8,$$

where the dimensionless value of R is 0.5. Thus, the value of ω decreases monotonically from a large positive value at the leading edge to 8 in the fully developed region.

Next, let us discuss the above deductions using the calculated results. The mesh system used is 1001×101, $\triangle X = 0.00001$, and $X \leq 0.01$. The pressure drop $\triangle p$ and pressure difference $(p_c - p_w)$ at $X \leq 0.01$ are listed in Table 4.4. The pressure difference $(p_c - p_w)$ across the radius of the pipe at $X \leq 0.002$ is shown in Figures 4.2 through 4.8. Here, the squares and circles denote the pressure drop $\triangle p_w$ at the wall and $\triangle p_c$ at the centerline, respectively.

Consider the pressure in the radial direction. For example, at Re = 1000, it is clear from Figure 4.4 (a) that (i) there is a large difference across the radius of the pipe between $\triangle p_w$ and $\triangle p_c$ at $X < 0.001$, and that this difference decreases as X increases.

Note that $\triangle p_w$ is larger than $\triangle p_c$. This indicates that (ii) the pressure p_w at the wall is lower than the pressure p_c at the centerline, i.e., that $p_w < p_c$. This difference contradicts results obtained by others via the boundary layer theory, and it also contradicts Bernoulli's law, although Bernoulli's law does not apply to viscous flow. In addition, it is seen from Figures 4.2 through 4.8 (a) that (iii) the difference $(p_c - p_w)$ decreases as Re increases. Values of $(p_c - p_w)$ are listed in Table 4.4, where we assumed that the $(p_c - p_w)$ values above approximately 0.01 are effective, as compared with $p_c - p_w = 0.089$ at Re = 2000 and

TABLE 4.4
Pressure drop at centerline ($\triangle p_c$) and pressure difference ($p_c - p_w$)

Re \ X	0.0001	0.0002	0.0003	0.0005	0.001	0.002	0.003	0.005	0.007	0.01
	Pressure drop at centerline ($\triangle p_c$)									
500	0.054	0.109	0.163	0.261	0.433	0.629	0.777	1.025	1.241	1.529
1000	0.074	0.144	0.204	0.290	0.421	0.606	0.756	1.008	1.224	1.514
2000	0.100	0.172	0.220	0.286	0.411	0.599	0.749	1.002	1.219	1.509
3000	0.115	0.179	0.220	0.284	0.410	0.597	0.748	1.001	1.218	1.508
5000	0.129	0.181	0.219	0.284	0.409	0.597	0.748	1.000	1.217	1.507
10000	0.134	0.181	0.220	0.284	0.409	0.596	0.747	0.999	1.216	1.505
	Pressure difference ($p_c - p_w$)									
500	0.435	0.308	0.236	0.142	0.040	0.006	0.002	0.0	0.0	0.0
1000	0.212	0.124	0.074	0.027	0.005	0.001	0.0	0.0	0.0	0.0
2000	0.089	0.030	0.011	0.003	0.001	0.0	0.0	0.0	0.0	0.0
3000	0.043	0.008	0.003	0.001	0.00	0.0	0.0	0.0	0.0	0.0
5000	0.012	0.001	0.0	0.0	0.0	0.0	0.0	0.0	0.0	0.0
10000	0.001	0.0	0.0	0.0	0.0	0.0	0.0	0.0	0.0	0.0
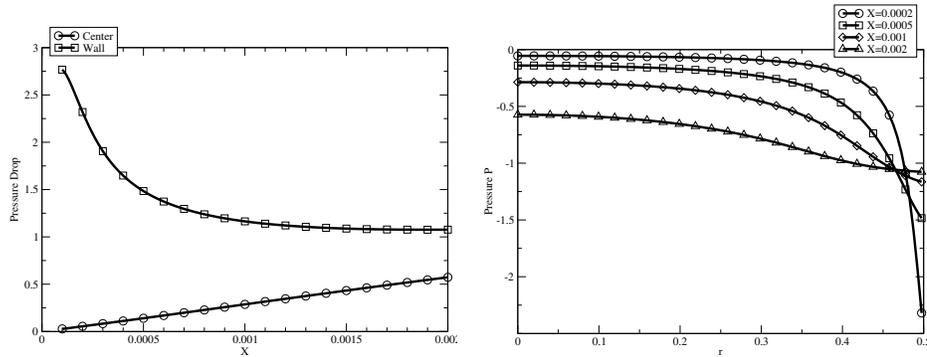
FIG. 4.2. *(a) Axial pressure drop and (b) pressure in r-direction, Re = 100.*

$X = 0.0001$: $p_c - p_w = 0.011 = 12\%$ of 0.089 at Re = 2000 and $X = 0.0003$; $p_c - p_w = 0.001$ $= 1.2\%$ of 0.089 at Re = 2000 and $X = 0.001$.

It is clear from Table 4.4 that at Re $\leq$ 2000 and $X = 0.0003$, there exists a significant pressure difference in the radial direction. Figures 4.2 through 4.8 (b) show the calculated results of the radial pressure distribution. At Re $\leq$ 1000, it is clear that (iv) the pressure gradient near the wall is higher than that at the central core. This indicates that (v) the pressure difference near the wall in the radial direction might be caused by NWS.

Note that the axial pressure distribution and Re are similarly related. Figure 4.9 illustrates the pressure drops at the wall and at the centerline for Re = 1000, 2000, and 3000. It is clear from Figure 4.9 that the difference ($p_c - p_w$) depends strongly on Re when Re $\leq$ 3000 near the inlet. Figure 4.9 and Table 4.4 also show that the pressure difference ($p_c - p_w$) disappears for $X \geq 0.001$ and Re $\geq$ 1000. More specifically (see Table 4.4), the pressure drop at the wall becomes the same as that at the centerline for $X \geq 0.0003$ and Re $\geq$ 3000. It is clear that at $X \geq 0.01$, the pressure drop at the centerline for Re = 500 becomes approximately the same as that for Re $\geq$ 1000 within a relative error of 1%.

In summary, there exists a large difference in pressure in the radial or normal direction near the inlet when Re = 2000 and X $\leq$ 0.0003. This pressure difference becomes negligible when Re increases beyond 10000. As discussed in Subsection 4.2, *Le* and $K(\infty)$ are approximately constant for Re $\geq$ 500. However, even when Re $\geq$ 500, the pressure difference ($p_c - p_w$) depends strongly on Re for Re $\leq$ 5000.

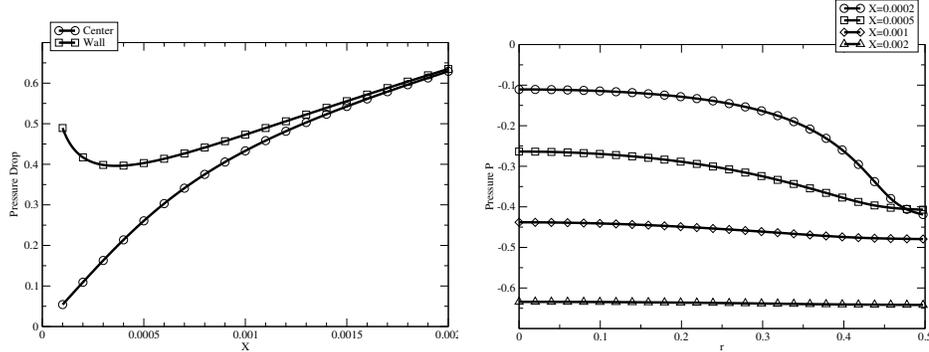We finally note that for an actual pipe of $D = 2.6$ cm and Re = 2000, $X = 0.0003$

FIG. 4.3. *(a) Axial pressure drop and (b) pressure in r-direction, Re = 500.*

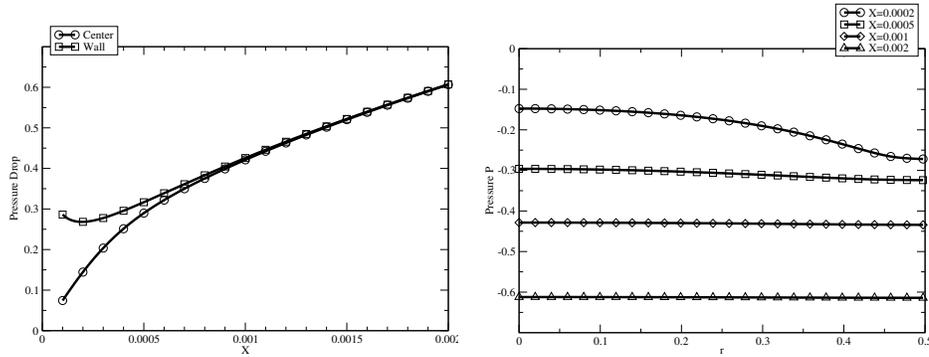

FIG. 4.4. *(a) Axial pressure drop and (b) pressure in r-direction, Re = 1000.*

indicates that the actual axial pipe length is $x' = 0.0003 \times 2.6 \times 2000 \approx 1.6$ cm. The radial pressure difference is effective over this length. Kanda's experiments [11] have shown that the critical Reynolds number is determined by the entrance shape of pipes, and a detailed numerical study is thus necessary for various entrance shapes of pipes. We also intend to study the relationship between NWS and the critical Reynolds number.

5. Conclusions. An analysis of flow development at Reynolds numbers from 500 to 10000 in the entrance region of a pipe was presented. In this study, the calculation procedure for pressure distribution was carried out without any preliminary assumptions. The Navier-Stokes equation can be expressed in vector form as (2.9). At the wall, the viscous term is expressed by the curl of vorticity so that the pressure gradient in the normal or radial direction is given by the vorticity gradient in the radial direction; see (2.10).

As a result, the radial pressure distribution was obtained for the first time for the above range of Reynolds numbers. The conclusions obtained can be summarized as follows.

1. The mesh systems from 21×21 to 201×201 are sufficient to calculate the velocity development, entrance length, and excess pressure drop, and the results agree well with those reported by previous researchers. However, with such meshes, we cannot see the radial pressure gradient. With refined meshes of $\triangle X < 0.0001$, we could determine the normal or radial pressure gradient for the first time.

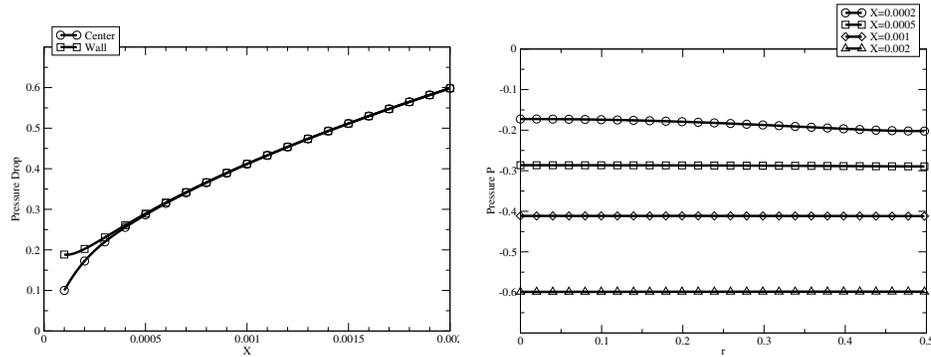2. There is a significant difference between p_w and p_c near the pipe inlet for

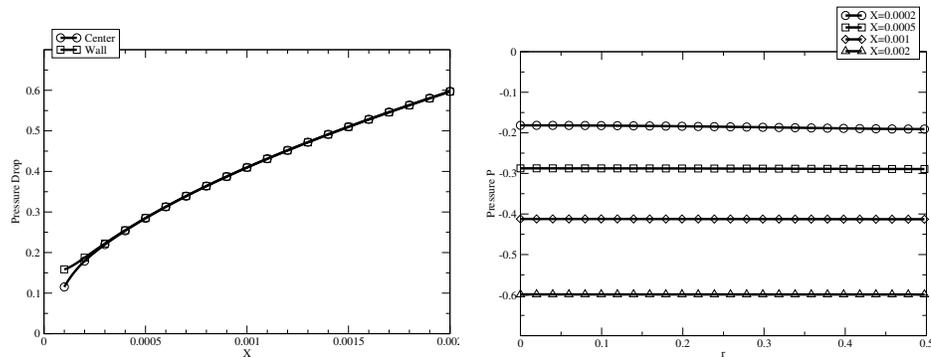FIG. 4.5. *(a) Axial pressure drop and (b) pressure in r-direction, Re = 2000.*

FIG. 4.6. *(a) Axial pressure drop and (b) pressure in r-direction, Re = 3000.*

Re $\leq$ 5000, where p_w is smaller than p_c. This contradicts the results obtained using the boundary layer theory, as well as Bernoulli's law, although the law does not apply to viscous flow. The difference between p_w and p_c disappears at Re $\geq$ 10000. This indicates that the boundary-layer assumptions hold for Re $\geq$ 10000. Note that NWS causes the difference $(p_w - p_c)$ and forces the fluid particles to move towards the centerline.

3. The calculated Le and $K(\infty)$ values are approximately the same at Re $\geq$ 500, respectively. Since the minimum critical Reynolds number is in the neighborhood of 2000, it is important to find a variable that varies at Re $\geq$ 500. We found that a pressure difference in the radial direction exists even when Re $\geq$ 500, and it varies inversely with increasing Re and disappears at Re $\geq$ 10000.

REFERENCES

[1] B. ATKINSON AND S. GOLDSTEIN, *Unpublished work described in Modern Development in Fluid Dynamics,* Dover, 1965, pp. 304–308.
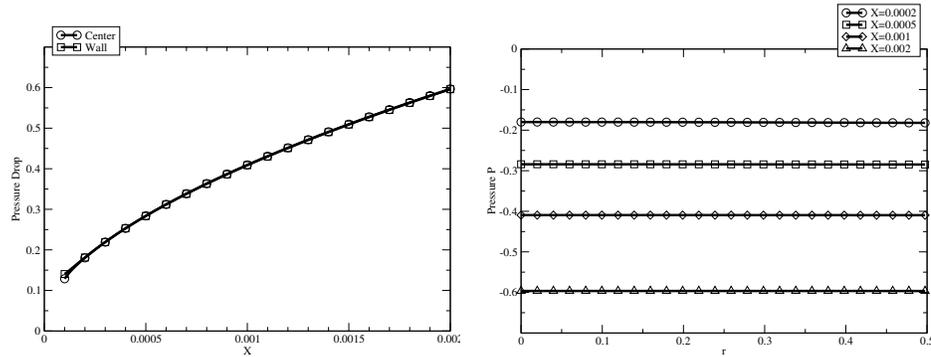
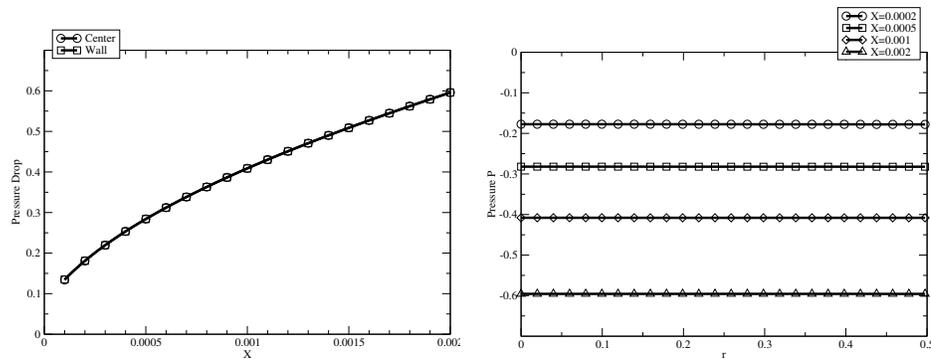FIG. 4.7. *(a) Axial pressure drop and (b) pressure in r-direction, Re = 5000.*

FIG. 4.8. *(a) Axial pressure drop and (b) pressure in r-direction, Re = 10000.*

[2] W. D. CAMPBELL AND J. C. SLATTERY, *Flow in the entrance of a tube,* ASME J. Basic Eng., Series D, 85(1) (1963), pp. 41–46.

[3] R.-Y. CHEN, *Flow in the entrance region at low Reynolds numbers,* J. Fluids Eng., 95 (1973), pp. 153-158.

[4] E. B. CHRISTIANSEN AND H. E. LEMMON, *Entrance region flow,* A.I.Ch.E. J., 11(6) (1965), pp. 995–999.

[5] F. DURST, S. RAY, B. UNSAL, AND O. A. BAYOUMI, *The development lengths of laminar pipe and channel flows,* J. Fluids Eng., 127 (2005), pp. 1154–1160.

[6] S. GOLDSTEIN, *Modern Developments in Fluid Dynamics, Vol. 1,* Dover, 1965.

[7] R. W. HORNBECK, *Laminar flow in the entrance region of a pipe,* Appl. Sci. Res., Sect. A, 13 (1964), pp. 224–236.

[8] H. KANDA, *Numerical study of the entrance flow and its transition in a circular pipe*, ISAS (The Institute of Space and Astronautical Science), Tokyo, Report No. 626, 1988.

[9] H. KANDA AND K. OSHIMA, *Radial pressure distribution for entrance flow in a circular pipe*, AIAA 36th Aerospace Sciences Meeting & Exhibit, AIAA 98-0792, 1998.

[10] H. KANDA, *Computerized model of transition in circular pipe flows. Part 2. Calculation of the minimum critical Reynolds number,* Proc. ASME Fluids Engineering Division-1999, ASME FED-Vol. 250 (1999), pp. 197–204.

[11] H. KANDA AND T. YANAGIYA, *Hysteresis curve in reproduction of Reynolds's color-band experiments,* Proc. 21st CFD (Computational Fluid Dynamics) Symp., JSFM (Japan Society of Fluid Mechanics), D3-1, 2007.

[12] H. L. LANGHAAR, *Steady flow in the transition length of a straight tube*, J. Appl. Mech., 9(2) (1942), pp. A55–A58.

[13] R. J. LEITE, *An experimental investigation of the stability of Poiseuille flow*, J. Fluid Mech., 5 (1942), pp. 81–96f.

[14] R. L. PANTON, *Incompressible Flow*, Wiley-Interscience, New York, 1984.

[15] R. PEYRET AND T. D. TAYLOR, *Computational Methods for Fluid Flow,* Springer, Berlin, 1983, p. 236.

[16] E. RESHOTKO, *Experimental study of the stability of pipe flow. I. Establishment of an axially symmetric*
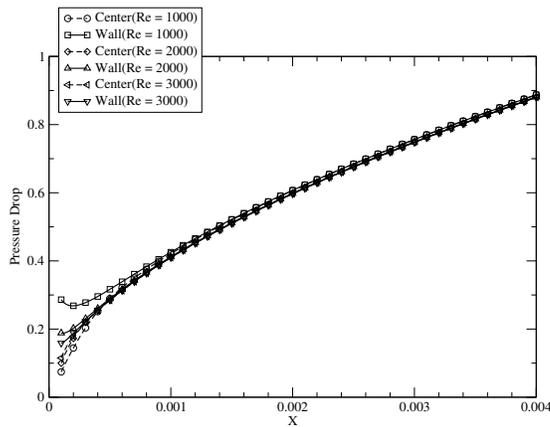
FIG. 4.9. *Axial pressure drop, Re = 1000 to 3000.*

Poiseuille flow, Jet Propulsion Lab., Pasadena, Progress Report No. 20-364, 1958.

[17] W. RIEMAN, *The value of the Hagenbach factor in the determination of viscosity by the efflux method,* J. American Chem. Society, 50 (1928), pp. 46–55.

[18] P. J. ROACHE, *Fundamentals of Computational Fluid Dynamics,* Hermosa, 1998, pp. 196–200.

[19] R. K. SHAH AND A. L. LONDON, *Laminar Flow Forced Convection in Ducts,* Academic Press, New York, 1978.

[20] K. SHIMOMUKAI AND H. KANDA, *Numerical study of normal pressure distribution in entrance flow between parallel plates, I. Finite difference calculations,* Electron. Trans. Numer. Anal., 23 (2006), pp. 202–218. http://etna.math.kent.edu/vol.23.2006/pp202-218.dir/pp202-218.html.

[21] S. TANEKODA, *Fluid Dynamics by Learning from Flow Images (in Japanese)*, Asakura Publishing Co., Tokyo, 1993, p. 165.

[22] J. S. VRENTAS J. L. DUDA, AND K. G. BARGERON, *Effect of axial diffusion of vorticity on flow development in circular conduits: Part I. Numerical solutions,* A. I. Ch. E. J., 12(5) (1966), pp. 837–844.

[23] Y. L. WANG AND P. A. LONGWELL, *Laminar flow in the inlet section of parallel plates,* A. I. Ch. E. J., 10(3) (1964), pp. 323–329.

[24] F. M. WHITE, *Fluid Mechanics*, Fourth ed., McGraw-Hill, New York, 1999, p. 260.